2018

Spinal cord organogenesis model reveals role of Flk1+ cells in self-organization of neural progenitor cells into complex spinal cord tissue

Baohan Pan
Johns Hopkins University

Hushan Ao
Washington University School of Medicine in St. Louis

Su Liu
Kennedy Krieger Inc.

Yuming Xu
Zhengzhou University

John W. McDonald
Johns Hopkins University

See next page for additional authors

Stem Cell Research 33 (2018) 156–165

Contents lists available at ScienceDirect

Stem Cell Research

journal homepage: www.elsevier.com/locate/scr

Spinal cord organogenesis model reveals role of Flk1$^+$ cells in self-organization of neural progenitor cells into complex spinal cord tissue

Baohan Pan[a,b], Hushan Ao[e,1], Su Liu[a], Yuming Xu[d], John W. McDonald[a,b,2], Visar Belegu[a,b,c,*,2]

[a] International Center for Spinal Cord Injury, Hugo W. Moser Research Institute at Kennedy Krieger Inc, Baltimore, MD, USA
[b] Department of Neurology, Johns Hopkins University School of Medicine, Baltimore, MD, USA
[c] Department of Pathology, Johns Hopkins University School of Medicine, Baltimore, MD, USA
[d] Department of Neurology, First Affiliated Hospital of Zhengzhou University, Zhengzhou 450052, China
[e] Center for the Study of Nervous System Injury and the Restorative Treatment and Research Center, Washington University School of Medicine, St. Louis, MO 63108, USA

ARTICLE INFO

Keywords:
Embryonic stem cells
Neural progenitor cells
Spinal cord organogenesis
Flk1

ABSTRACT

A platform for studying spinal cord organogenesis *in vivo* where embryonic stem cell (ESC)-derived neural progenitor cells (NPC) self-organize into spinal cord-like tissue after transplantation in subarachnoid space of the spinal cord has been described. We advance the applicability of this platform by imaging *in vivo* the formed graft through T2*w* magnetic resonance imaging (MRI). Furthermore, we used diffusion tensor imaging (DTI) to verify the stereotypical organization of the graft showing that it mimics the host spinal cord. Within the graft white matter (WM) we identified astrocytes that form glial limitans, myelinating oligodendrocytes, and myelinated axons with paranodes. Within the graft grey matter (GM) we identified cholinergic, glutamatergic, serotonergic and dopaminergic neurons. Furthermore, we demonstrate the presence of ESC-derived complex vasculature that includes the presence of blood brain barrier. In addition to the formation of mature spinal cord tissue, we describe factors that drive this process. Specifically, we identify Flk1$^+$ cells as necessary for spinal cord formation, and synaptic connectivity with the host spinal cord and formation of host-graft chimeric vasculature as contributing factors. This model can be used to study spinal cord organogenesis, and as an *in vivo* drug discovery platform for screening potential therapeutic compounds and their toxicity.

1. Introduction

Spinal cord is derived from embryonic stem cells (ESCs) through a coordinated organogenesis. Formation of the neural tube and subsequent expansion of the neuroepithelium gives rise to neural progenitor cells (NPCs) that further differentiate into multiple cell lineages that form the brain and spinal cord (Aiba et al., 2006; Edlund and Jessell, 1999). Cellular diversity of the central nervous system (CNS) depends on highly regulated cell fate decisions (Edlund and Jessell, 1999). In addition to NPCs, a subpopulation of the cells that express Flk1, also known as vascular epithelial growth factor (VEGF) receptor 2, has been suggested to play a role in early neurogenesis. Flk1 induction has been demonstrated in ESC-derived NPCs and in NPCs of adult mouse brain (Jin et al., 2002a; Schanzer et al., 2004a; Shen et al., 2004). Flk1$^+$ cells go on to differentiate into neural and endothelial precursors (Clarke et al., 2000; Tropepe et al., 2001). While Flk1$^+$ cells are critical for vasculature development (Kabrun et al., 1997), their role in CNS organogenesis remains unclear.

The ability of ESCs to differentiate into cells with a wide array of molecular phenotypes makes them good candidates in therapeutic interventions. *In vitro*, ESCs have been shown to differentiate into cells that constitute several tissue types including, blood and blood vessels, heart, muscle, and CNS (Bjorklund et al., 2002; Doevendans et al., 2000; Kaufman et al., 2001; Klug et al., 1996; Lee et al., 2000; Lumelsky et al., 2001; Palacios et al., 1995; Wichterle et al., 2002; Yamashita et al., 2000). In addition to clinical utility, ESC-derived tissues provide a platform for studying mechanisms that regulate organogenesis and regeneration. Toward this, ESCs have been used to generate complex tissue such as cortical tissue, retina and pituitary gland (Eiraku and Sasai, 2012; Eiraku et al., 2011; Suga et al., 2011), cerebral organoids

Abbreviations: ESC, embryonic stem cells; NPC, neural progenitor cells; T2*w*, *T2-weighted*; DTI, diffusion tensor imaging; WM, white matter; GM, grey matter

* Corresponding author: International Center for Spinal Cord Institute, Hugo W. Moser Research Center at Kennedy Krieger Inc, 707 N. Broadway, Baltimore, MD 21205, USA.
E-mail address: vbelegu@gmail.com (V. Belegu).
[1] Current address: Department of Anesthesiology, Chinese Academy of Medical Sciences and Peking Union Medical College Fuwai Hospital, Beijing, 100037, China.
[2] Co-senior authors.

https://doi.org/10.1016/j.scr.2018.09.001
Received 26 July 2017; Received in revised form 2 August 2018; Accepted 5 September 2018
Available online 06 September 2018

(Lancaster et al., 2013), and the patterned neural tube formation (Meinhardt et al., 2014). While the formation of mature spinal cord tissue has not been reported *in vitro*, there is one report showing formation of such tissue *in vivo* (Ao et al., 2011).

Here, in a model of spinal cord organogenesis (Ao et al., 2011), we show that formation of self-organized tissue from ESC-derived NPCs can be imaged *in vivo* with T2*w* MRI while the stereotypical organization of the graft can be discerned by DTI. We also demonstrate that complex features of the spinal cord are found within the graft. In validation of the ability of this platform to study intrinsic molecules of ESCs that drive spinal cord organogenesis, we show that Flk1$^+$ cells are necessary for the formation of the graft following transplantation ESC-derived NPCs.

2. Material and methods

2.1. Cell culture

B5 mouse ESCs (from Dr. Andras Nagy) that express GFP ubiquitosusly were cultured as previously described (Bain et al., 1995;McDonald et al., 1999a). Briefly, undifferentiated ESCs were propagated in the presence of leukemia inhibitory factor (LIF; Life Technologies). Cells were cultured as EBs in ESC induction medium (ESIM; described by Bain et al. (Bain et al., 1995)) for 4 days, and then treated for 4 days with retinoic acid (all-trans-RA, 500 nM; Sigma Aldrich) (Bain et al., 1995). On the ninth day, EBs were dissociated with 0.25% trypsin plus EDTA (5 min at 37 °C). The resulting single-cell NPCs were resuspended in ESIM, and transplantated or depleted of Flk1$^+$ cells. A source of dead ESCs were produced by repeated freeze thaw cycles (see sham group below). We confirmed the lack of viable ESCs by the presence of trypan blue in the cells used for transplantation in the sham group.

2.2. Depletion of Flk1$^+$ cells by complement cascade, and inhibition of Flk1 signaling

Dissociated ESC-derived NPCs (2×10^6cells/mL) were treated with rat monoclonal anti-Flk1 IgG at 1:50 or normal rat IgG for 20 min, followed by rabbit complement at 1:25 or normal rabbit serum for 45 min. Cells were washed, and reconstituted for transplantation in ESIM at 1 × 106 cells/mL. In addition, batches of ESC-derived cells were treated with 1 mM ZM323881 (Santa Cruz Biotech), a specific Flk1 inhibitor(Xiao et al., 2007), from day 2 to day 8. We measured the diameter of EB spheres treated with ZM323881.

2.3. Animals

All surgical procedures and animal care were done in compliance with Animal Studies Committee of Washington University in St Louis School of Medicine and Johns Hopkins University IACUC. Female Long-Evans rats (200–220 g) were housed in 12 h light/dark cycle with *ad libitum* access to food and water.Table 1summarizes the groups of animals used in this study.

Table 1
Summary of cell dosage and animal groups.

Injection dose (millions of cells)	Number of animals in the group	Number of animals with graft growth	Ratio of animals with graft (%)	Median BBB score
0	3	0	0	21
2.5	8	3	37.5	21
5	12	6	50	21
10	10	4	40	21
20	13	7	54	21
40	24	16	66.7	21

2.4. Transplantation, treatment and control groups

We transplanted ESC-derived NPCs at five different doses 5, 10, 20, or 40 million. Three animals constituted a sham group that was transplanted with dead ESCs. The freeze-thaw cycle used to generate dead ESCs was started with 40 million cells. In the depletion of Flk1$^+$cells by complement cascade experiment the control group was transplanted with B5 ESC-derived NPCs while the experimental group was transplanted with Flk1$^+$depleted B5 ESC-derived NPCs. Animals were anesthetized with ketamine/medetomidine (75,0.5 mg/kg i.p.). Laminectomy was performed in anesthetized animals at L5–6 and cells were injected into the L5–6 subarachnoid space. Anesthesia was reversed with antipamezole (1.0 mg/kg s.c.). All animals received immunosuppression (cyclosporine, 10 mg/kg, s.c.) starting 24 h prior to the transplantation, and daily thereafter. Animals were perfused with 4% paraformaldehyde in 0.1 M PBS. Spinal cord was dissected, and post-fixed for 2 h. Spinal cord tissue was examined for GFP expression with a fluorescent dissection microscope to assess ESC-derived graft. Three of the spinal cords were further processed for *ex vivo* MRI. Other spinal cords were cryoprotected in 30% glucose overnight, frozen and sectioned at 14 μm at transverse or longitudinal plane. Relationship between the number of transplaned cells and graft formation was analysed by linear regression analysis with Prism 6 (GraphPad Software).

2.5. In vivo MRI

At 2.5 months after transplantation, 10 animals were anesthetized with 2% isoflurane, received *in vivo* MRI scans to assess graft formation. The animals that received *in vivo MRI scans were transplanted with 40 million cells.* Scans were performed in a horizontal 9.4 T NMR spectrometer (Bruker; maximum gradient strength imaging = 400mT/m. Images were acquired with a 70-mm diameter volume coil as the radio frequency transmitter and receiver. T2*w* images covering the entire lumber sacral spinal cord were acquired with rapid acquisition with refocused echoes (RARE) sequence with the following parameters: TE = 30 ms, TR = 4600 ms, echo train length = 4, four signal averages, FOV = 51.3 mm × 51.3 mm, 2 mm slice thickness, and an in-plane resolution of 0.27 mm × 0.40 mm. Seven out of the 10 animals that were imaged using *in vivo* MRI formed grafts.

2.6. ex vivo MRI

Ex vivo scans were performed in a vertical 11.7 T NMR spectrometer (Bruker) equipped a 10-mm diameter volume coil as the radio frequency transmitter and receiver. DTI data were acquired using the diffusion weighted 3D GRASE sequence with the following parameters: TE of 33 ms, TR of 800 ms, and 4 signal averages. The imaging FOV, and matrix size were 10.0 mm × 8.0 mm × 11.0 mm and 128 × 96 × 180 respectively, and the native resolution was 78 × 84 × 60 mm^3. The spectral data were apodized by a symmetric trapezoidal function with 10% ramp widths on either side of the trapezoid and zero-filled before Fourier transformation. For DTI, six diffusion weighted images (b-value 1700 s/mm^2) and two non diffusion-weighted images were acquired with d = 3 ms, D = 15 ms. Signal-to-noise ratios in the spinal cord in non-diffusion weighted images were > 40. Diffusion tensors were calculated using a log-linear fitting method. Maps of fractional anisotropy (FA) were calculated on a voxel-by-voxel basis from the diffusion tensor using DTIStudio (Jiang et al., 2006).

2.7. Neuronal tract tracing with pseudorabies virus (PRV)

Four days prior to experimental endpoint, 7 animals that received ESC-derived NPCs were anesthetized with isoflurane. The left sciatic nerve was exposed, and we performed a 2-μL intra-nerve injection of the Bartha strain of PRV (1×10^8 PFU/mL, provided by Dr. Lawrence

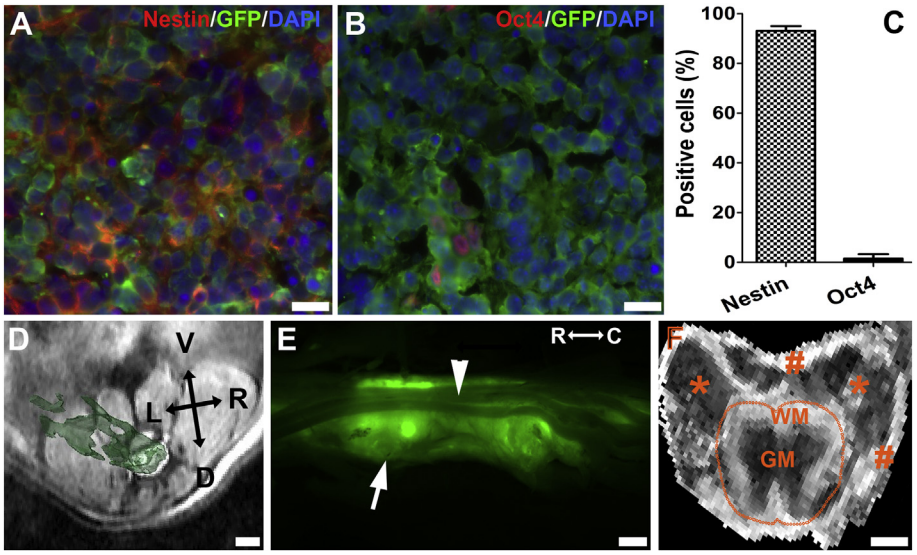

Fig. 1. Presence and stereotypical self-organization of intrathecally transplanted ESC-derived NPCs can be ascertained by MRI. (A) Differentiation of ESCs into NPCs prior to transplantation is confirmed by expression of nestin, a marker of NPCs (2825 cells were counted from 6 EBs; 93.07 ± 1.96% of cells expressed nestin). (B) Prior to transplantation ESC-derived NPCs do not express Oct4, a marker of pluripotent stem cells (4970 cells were counted from 10 EBs; 1:55 ± 1:96% of counted cells express Oct4). (C) Quantification of nestin$^+$ and Oct4$^+$ cells in panels A and B, respectively. (D) *In vivo* T2*w* image with a 3D reconstruction of the graft (green); V, ventral; C, caudal; L, left; R, right. (E) Segments of the lumbosacral cord illustrate GFP-fluorescence around the host spinal cord (white arrows point at the graft, white arrowhead points at the spinal roots); R, rostral; C, caudal. (F) FA map, from L5-L6 level of the spinal cord, illustrates the relationship between host and graft tissue highlighting the inside-out stereotypical self-organization of graft (white matter, WM; grey matter, GM; orange *, graft GM-like tissue; orange #, graft WM-like tissue; dotted orange circles, spinal cord). Scale bars A-B = 15 μm; D-F = 0.5 mm. (For interpretation of the references to colour in this figure legend, the reader is referred to the web version of this article.)

Schramm). The muscle and skin incisions were closed separately. Animals injected with PRV were allowed to survive for 90 h (Pan et al., 2005).

2.8. Immunohistochemistry

For neuron labeling we used antibodies against: choline acetyltransferase (ChAT, Millipore); vesicular glutamate transporter 1 (vGlut1, Millipore); hydroxytryptamine (5-HT, Millipore); tyrosine hydroxylase (TH, Millipore). Oligodendrocytes: myelin basic protein (MBP, Dako). Astrocytes: glial fibrillary acidic protein (GFAP, Incstar). Vasculature: Flk1 (BD), and CD31 (Dako). Transplanted cells were identified with anti-green fluorescent protein (GFP). For PRV infected neurons, a swine polyclonal anti-PRV antibody was used (provided by Dr. Arthur Loewy). Corresponding secondary antibodies conjugated with Alexa 488, Cy3 or Cy5 were used (Jackson Immunoresearch), and sections were counterstained with Hoechst 33342 (Molecular Probes).

2.9. Quantitative image analysis

For quantification, images were captured on a Zeiss Axio Imager Z1 microscope (Zeiss). Mean fluorescence intensities for ChAT$^+$ neurons, vGlut1$^+$, 5HT$^+$, and TH$^+$ axons from a region of interest (ROI) from the host spinal cord and the graft were obtained with Zeiss Zen 2012 software for measuring signal intensity (Zeiss). Mean fluorescence intensities are reported for ROIs obtained from three animals, and *t*-test was used for comparison of neuronal markers with Prism 6 (GraphPad Software). In this work, we use the mean fluorescence intensities for each neuronal marker as a correlate for the number of the respective neurons.

2.10. Electron microscopy (EM)

Spinal cord and ESC cell graft were processed using standard methods (Liu et al., 2000). Tissue was trimmed and postfixed in osmium, and embedded in Epon. Thin sections were obtained and stained for citrate/uranyl acetate. Electron micrographs were acquired using a JEOL 100CX transmission EM.

3. Results

Self-organization of transplanted ESC-derived NPCs into spinal cord-like tissue is independent of the number of transplanted cells.

Mouse ESCs were differentiated into NPCs by removal of leukemia inhibitory factor (LIF) and subsequent addition of retinoic acid (RA) (Bain et al., 1995). After 4 days without LIF, and another 4 days in the presence of RA, mouse ESCs-derived NPCs predominantly expresses nestin (98.45 ± 1.96%, n = 2825), an NPC marker. Mouse ESC derived cells did not express Oct4 (1.55 ± 1.96%, n = 4970, a marker of undifferentiated ESCs (Fig. 1A–C). Previously, transplantation of 50 million mouse ESC-derived NPCs in the subarachnoid space showed formation of mature neuronal tissue that resembles the spinal cord (Ao et al., 2011). To determine if the ability of ESCs-derived NPCs to self-organize depends on the number of transplanted cells, we transplanted a lower number of ESC-derived NPCs into the subarachnoid space at lumbosacral level of adult rat spinal cord; specifically, we transplanted 2.5, 5, 10, 20, and 40 million cells. In an attempt to streamline the characterization of the grafts for future studies, we screened the lumbosacral spinal cords for the formation of ESC-derived grafts using *in vivo* T2*w* MRI (Fig. 1D) in 10 animals that were transplanted with 40 million cells (7 animals in this cohort formed grafts). The rostro-caudal dimension of the grafts ranged from 0.2 mm to 25 mm (Fig. 1E). Transplantation of all five doses of ESC-derived NPCs resulted in graft formation. In total, 36 out of 67 transplanted animals had grafts (Table 1) whereas no grafts were observed in animals transplanted with dead NPCs. We used linear regression analysis to determine if number of transplanted cells, the common independent variable, can predict the ability of the transplanted cells to form grafts, the dependent variable. Based on the values of coefficient of determination (R^2 = 0.5618) and its corresponding p value (p = .0862) we concluded that the formation of the grafts does not depend on the number of cells that are transplanted (Supplementary Fig. S1 visualizes the linear regression analyses from data in Table 1). In addition, transplantation of various numbers of mouse ESC-derived NPCs did not lead to teratomas.

Next, we utilized DTI to investigate the organization of the transplanted ESC-derived NPCs. Diffusion of water within highly organized graft structure should be limited to the same extend as it is in the host spinal cord reflecting similarities in fiber density, axon diameter and myelination. Indeed, FA maps show that the spatially distinct areas within the graft grossly resemble WM and GM tissue of the host spinal cord (Fig. 1F). In addition, FA maps also show that the self-organization of the graft reconstitutes the stereotypical inside-out organization of the mature spinal cord (Fig. 1F).

All the transplanted animals had normal gait achieving a perfect

score on the Basso, Beattie and Bresnahan (BBB) open-field locomotor test (Table 1) (Basso et al., 1995), and exhibited no signs of pain or discomfort (signs of discomfort that were monitored where vocalization when handled, decreased body weight, poor grooming, and reduction in free movement).These findings demonstrate that as few as 2.5 million transplanted ESC-derived NPCs self-organize in tissue whose gross architecture closely resembles the normal spinal cord without compromising the host spinal cord. In addition, T2*w* MRI can be used to assess graft formation in live animals making this spinal cord organogenesis model more applicable for developmental and toxicology studies.

3.1. Principal cellular components within the ESC-derived graft are functional

Previous investigation showed that ESC-derived grafts contain neurons, astrocytes and oligodendrocytes, three principal components of the CNS (Ao et al., 2011). We aimed to examine the functionality of these components; therefore, we examined functional and anatomical features formed by neurons, oligodendrocytes and astrocytes. Toward this, we first probed the interaction of oligodendrocytes and neurons within the graft WM where we found that MBP^+ myelin sheaths wrap NFT^+ axons (Fig. 2A-B). Indeed myelination of axons within the graft leads to the formation of Caspr+ paranodal structures, a component of the machinery that enables saltatory conduction (Fig. 2A and C) (Einheber et al., 1997a). An illustrative electron micrograph of the WM within the graft confirms the formation of paranodes adjacent to myelin sheaths (Fig. 2D). In addition, the presence of compact myelin sheaths enwrapping axons corroborates the functionality of interactions between oligodendrocyte and neurons in the graft WM (Fig. 2D). Myelination by ESC-derived oligodendrocyte in the graft resembles myelination of larger diameter axons by host oligodendrocytes. The graft also contains unmyelinated axons (Fig. 2D), and we do not observe myelination of dendrites or non-neuronal cell processes.

Second, we aimed to show that the previously described dense outer zone of radial astrocytes in the graft WM forms a glial limitans (Alghamdi and Fern, 2015). Electron micrograph illustrated in Fig. 2E depicts the soma of a highly ramified astrocyte with glial filaments that the astrocyte contributes to the glial limitans. The astrocyte illustrated in Fig. 2E ensheaths several axons within the graft WM. Presence of tight junctions in the dense outer zone populated by astrocytes confirmed the formation of the glial limitans in the graft WM (Fig. 2E, E inset). Finally, in an area adjacent to host spinal roots, we observed morphology features strongly resembling transitional zones that are characteristic of the dorsal root entry zones (Fig. 2A and F). In these zones, PNS patterns of myelination, characterized by myelinating Schwann cells (Fig. 2F) with adjacent collagen fibers (Fig. 2F), transition into CNS-like patterns of WM, characterized by axons and oligodendrocyte (Fig. 2F). The presence of functional and anatomical features formed by the three principal neural cells within the graft supports the notion that these cells are functional, and validate this platform as a model for spinal cord organogenesis.

3.2. Molecular phenotypes of ESC-derived neurons resemble spinal cord neurons

Having shown that the stereotypical inside-out organization of the graft resembles the spinal cord, and that the three principal neural components within the graft are functional, we aimed to determine if the molecular phenotypes of ESC-derived neurons within the graft resemble neurons found in the host spinal cord (Fig. 3A). First, we examined expression and distribution of ChAT, a marker of cholinergic neurons, in the graft. Cholinergic neurons in the graft appear in clusters and possess large processes (Fig. 3B) resembling cholinergic motor neurons found in the host spinal cord ventral horn, as seen within the same section (Fig. 3B). In addition to the distribution, we aimed to

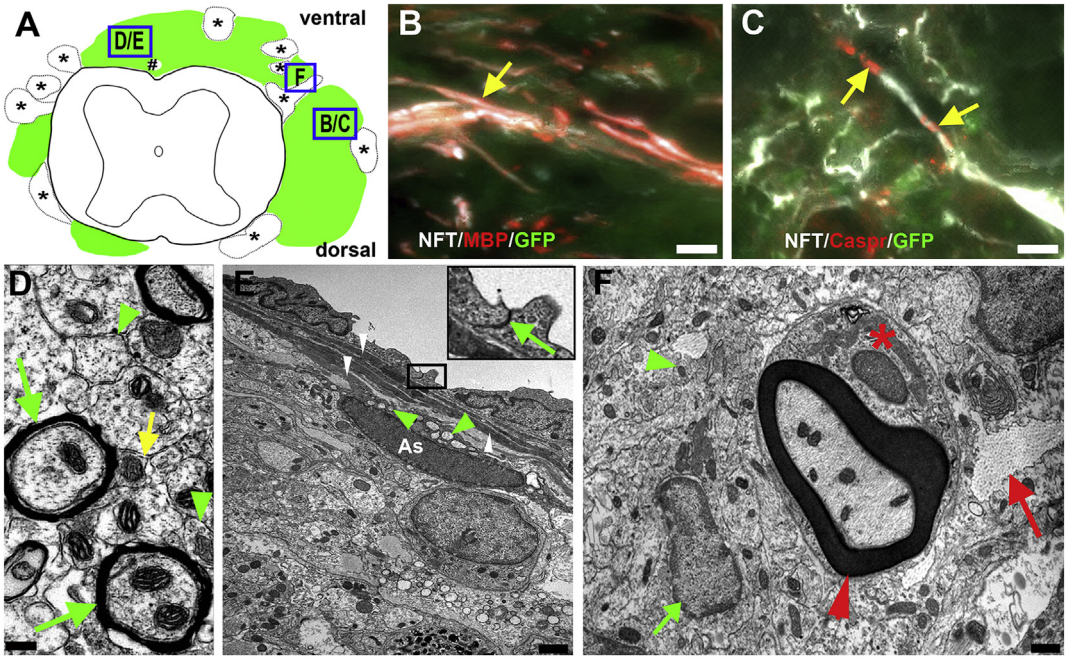

Fig. 2. (A) Schematic diagram of a coronal section of the lumbar spinal cord with the graft (green) where the letters correspond to individual panels (B–F) (*, nerve roots; #, anterior spinal artery). (B) MBP (red) and NFT (white) labeling illustrates myelin wrapped axons in the graft (yellow arrow). (C) Myelinated axons (NFT, white) form paranodal structures (yellow arrow, paranodes). (D) EM micrograph within the WM tissue of the graft shows oligodendrocytes myelination of axons is developmentally appropriate (green arrows, myelin sheaths; green arrowheads, unmyelinated axons; and yellow arrow, paranodes). (E) The external surface of the graft depicts a glial limitans with tight junctions between cells on the surface (inset, green arrow) (As, astrocyte; white arrowheads, astrocyte processes; green arrowheads, axons ensheathed by astrocyte processes). (F) The graft-host interface resembles the dorsal root entry zone with myelinating Schwann cells (red *, cell body; red arrowhead, myelin sheath), collagen (red arrow), oligodendrocytes (green arrow, cell body) and axons (green arrowhead). Scale bars: B-C = 10 μm; D = 0.2 μm; E = 2 μm; F = 0.5 μm.

assess the quantity of each neuronal phenotype by using the intensity of immunofluorescence for each marker as a correlate for the number of neurons. Initially, we assessed the quantity of cholinergic neurons by ChAT immunofluorescence (Supplemental Fig. S2A). We found that the number of cholinergic neurons found within the graft (4166 ± 227) is lower than in the host spinal cord (5621 ± 346; $p < .01$). Second, we examined expression of vGlut1, a marker of glutamatergic neurons in the graft (Fig. 3C). Glutamatergic neurons with numerous vGlut1 bouton-like terminals are found in the graft GM, and they resemble glutamatergic profiles in the dorsal horn of the host spinal cord (Fig. 3D). Unlike cholinergic neurons, the number of glutamatergic neurons, assessed by vGlut1 immunofluorescence (Supplemental Fig. S2B), within the graft (9894 ± 474) is higher than in the host spinal cord (6992 ± 347; p <001). Third, we examined expression of 5-HT (Fig. 3E), a marker of serotonergic neurons, and TH (Fig. 3G), a marker of dopaminergic neurons, in the graft. Serotonergic and dopaminergic neurons are found in the graft GM and have numerous terminals with bouton-like structures that are 5-HT$^+$ (Fig. 3E) and TH$^+$ (Fig. 3G), respectively, resembling serotonergic (Fig. 3F) and dopaminergic (Fig. 3H) neurons of the host spinal cord. The number of serotonergic neurons, assessed by 5-HT immunofluorescence (Supplemental Fig. S2C) is lower in the graft (2523 ± 56) than in the host spinal cord (3892 ± 73, $p < .001$) while the number of dopaminergic neurons, assessed by TH immunofluorescence (Supplemental Fig. S2D), is higher in the graft (6028 ± 161) than in the host spinal cord (5537 ± 94, $p < .01$). Therefore, similarities in the presence, appearance, and distribution of ESC-derived ChAT$^+$, vGlut1$^+$, 5-HT$^+$, and TH$^+$ neurons in the graft confirm that neuronal molecular phenotypes from the graft are very similar to neurons in the host spinal cord whereas the quantity of these markers highlights the variability in the numbers of neurons in graft *versus* the host spinal cord. Such variability could be a consequence of the selection of ROIs within the same transverse version of the host spinal cord, and could be different in other levels of the graft. For example, the number of glutaminergic neurons in one level of the graft could resemble the number of glutaminergic neurons at a different level of the host spinal cord. Alternatively the variability could be due to differences in developmental cues in the adult host spinal cord *versus* within the graft.

3.3. Astrocyte migration and neuronal connectivity can provide cues for spinal cord organogenesis

The similarity of the molecular phenotypes between neurons of the host spinal cord and ESC-derived neurons within the graft prompted us to examine interactions between the graft and the host spinal cord. Initially, we examined the interface between the graft and the host where we find ESC-derived neurons (NeuN$^+$/GFP$^+$) that migrate into the host spinal cord (Fig. 4A), and host neurons (NFT$^+$/GFP$^-$) that project axons into the graft (Fig. 4B). Additionally, at the interface we found that host astrocytes (GFAP$^+$/GFP$^-$) migrate into the graft (Fig. 4C). The finding that host neurons project their axons into the graft introduces the possibility that host and graft neurons form neuronal networks. For a more detailed assessment of connectivity between the neurons in the host and graft, we injected transsynaptic retrograde tracer PRV in the sciatic nerve. We found PRV$^+$ neurons in the GM of the host spinal cord at the caudal lumbosacral level (Fig. 4D–E). Additionally, we found PRV$^+$ neurons scattered in the GM of the graft suggesting that the neurons in the graft form synaptic neuronal circuits with the host spinal cord neurons (Fig. 4D–F″). Taken together – the presence of host astrocytes within the graft, and formation of circuitry between the host and graft neurons – these results allow the possibility that the host CNS plays an active role in directing spinal cord organogenesis within the graft.

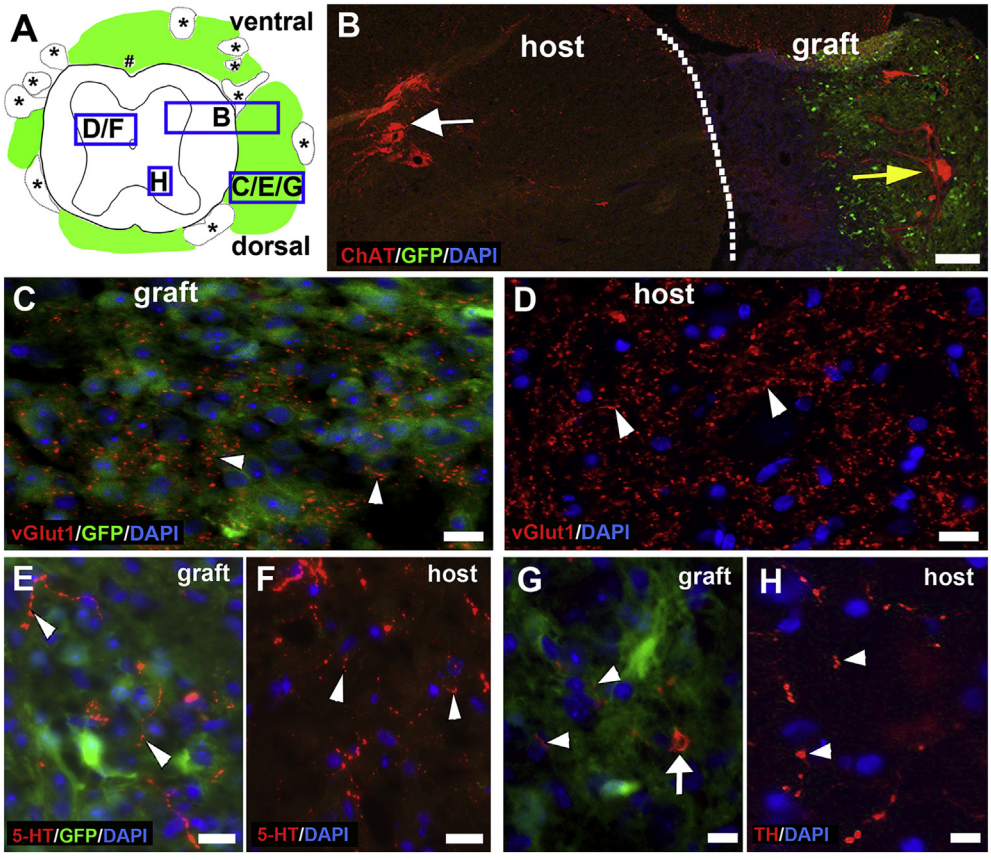

Fig. 3. Molecular phenotypes of neurons in the graft resemble neurons in the host spinal cord. (A) Schematic drawing through the lumbar spinal cord showing letters that correspond to the locations of panels B—H (*nerve roots, # anterior spinal artery). (B) Ventral horn of the host spinal cord and the graft contain clusters of ChAT+ cholinergic neurons (white arrow, ChAT$^+$ neurons in the spinal cord; yellow arrow, ChAT$^+$ neurons in the graft; white dotted line, graft-host boundary). (C-D) vGlut1 labeling graft GM shows dense glutaminergic nerve terminals in the graft (C), similar to that in the ventral horn of the host spinal cord (D). (E-F) 5-HT labeled axons (arrowhead) in the graft GM (E) resemble those in the ventral horn of the host spinal cord (F). (G-H) Similarly, TH$^+$ axons (arrowhead) in the graft GM (G; arrow highlights the cell body of a TH$^+$ dopaminergic neuron) are similar to those in the ventral horn of the host spinal cord (H). Scale bars B = 50 μm; C-H = 10 μm.

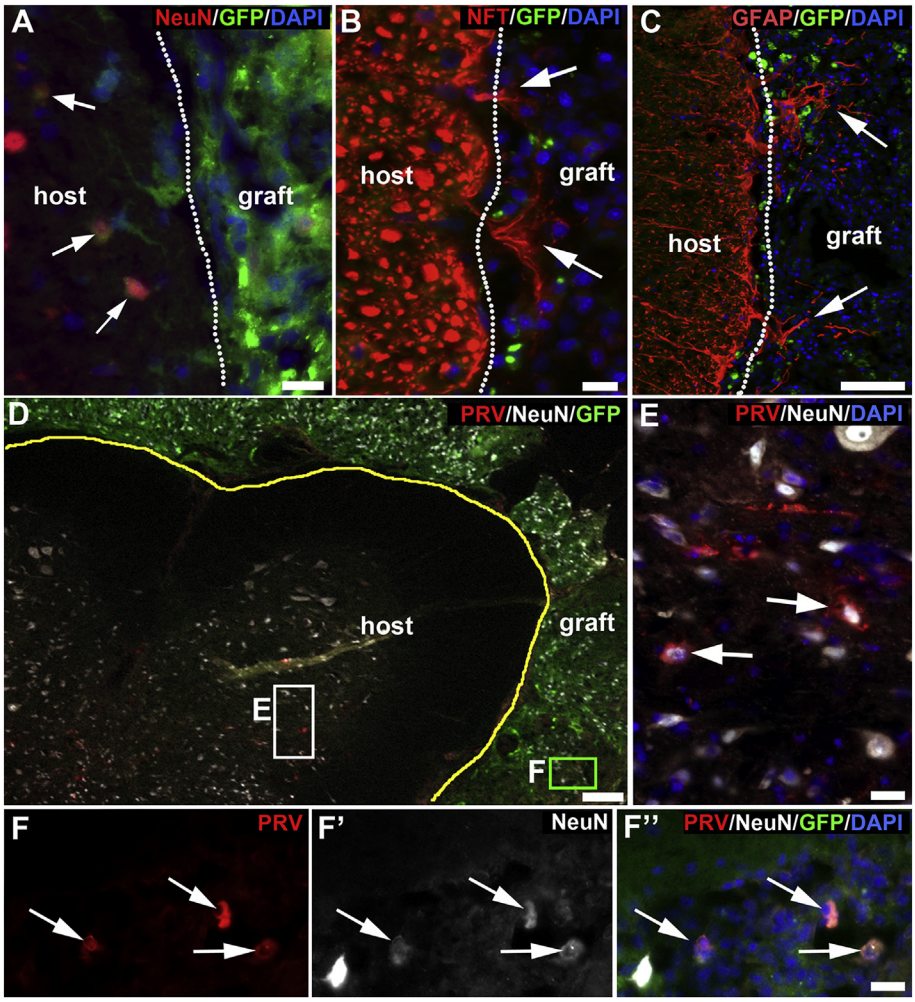

Fig. 4. Neural connections between the host spinal cord and graft. (A) GFP$^+$NeuN$^+$ cells (arrows) from the graft migrate into the host spinal cord (white dotted line, graft-host boundary). (B) NFT$^+$ neurons from the host spinal cord (arrows) project axons in the graft. (C) GFAP$^+$ astrocytes from the host spinal cord (arrows) migrate into the graft. (D) Pseudo-rabies virus (transynaptic retrograde tracer) injected in the sciatic nerve labels neurons in the GM of the host lumbosacral spinal cord and the graft showing that neurons from the graft form functional synaptically connected circuitry with neurons in the host spinal cord (yellow line in D, graft-host boundary). (E) Inset from panel D (white box) showing PRV-labeled (red) NeuN$^+$ neurons (arrows) in the GM of the host spinal cord. (F-F″) Inset from panel D (green box) showing ESC-derived (GFP$^+$) PRV-labeled (red) NeuN$^+$ neurons (arrows) in the GM of the graft. Scale bars: A-C = 50 μm, D = 100 μm, E-F″ = 20 μm.

3.4. Formation of vasculature in the graft

Vasculogenesis and angiogenesis are essential for organogenesis since they enable oxygen and nutrient exchange, and they provide instructive signals to non-vascular tissue during organ development. Therefore, we wanted to determine the level of vasculogenesis or angiogenesis within the graft as well as the role they play in the process of spinal cord organogenesis. First, we examined expression of Flk1, an early endothelial marker (Kabrun et al., 1997; Yamashita et al., 2000; Yamaguchi et al., 1993). Flk1$^+$/GFP$^+$ cells were identified as individual cells (Fig. 5A) and as part of vasculature within the graft (Fig. 5B). In addition, we found Flk1$^+$ vasculature that ran continuous between the host and the graft (Fig. 5C) indicating that the vasculature within the graft is chimeric. Formation of chimeric vasculature that is shared between the host and the graft introduces another avenue through which the host spinal cord can play a role in directing spinal cord organogenesis within the graft. Second, we examined the expression of a mature endothelial marker, CD31 (Fig. 5D). Unlike Flk1$^+$ cells, we only find CD31$^+$ cells within the graft vasculature. The presence of CD31$^+$/GFP$^+$ cells indicates that the mature vasculature that forms within graft originates from the transplanted cells. Third, we examined expression of Glut1, a marker of endothelial cells that comprise the blood-brain barrier (Fig. 5E). The presence of GFP$^+$Glut1$^+$ cells in the vasculature of the graft indicates vasculogenesis initiated from the transplanted cells has resulted in complex vasculature that includes elements of CNS vasculature such as blood-brain-barrier (Fig. 5E) that also contain tight junctions (Fig. 5F–F′) (Engelhardt, 2003; Kuhnert et al., 2010). Taken together these findings show that transplanted ESC-derived cells initiate the process of vasculogenesis that results in complex vasculature within the graft including the presence of the blood-brain-barrier. Additionally, the chimeric nature of the vasculature within the graft shows that angiogenesis from the host contributes to the vasculature within the graft possibly influencing spinal cord organogenesis in the graft.

3.5. Flk1$^+$ cells regulate embryoid bodies (EB) growth and graft formation

Following the observation that ESC-derived cells are part of the vasculature within the graft, we wanted to determine if ESC-derived Flk1$^+$ cells are present in the EB, and if Flk1 regulates EB growth. Toward this, we determined that at day 8 of EB growth, Flk1$^+$ cells constitute 6.9 ± 0.9% (total cells counted 21,005) of cells within EB. Subsequently, we grew EBs in the presences of ZM323881 (1 μM), a specific inhibitor of Flk1 kinase activity (Fig. 5G–I) (Xiao et al., 2007). Inhibition of the Flk1 signaling resulted in EBs that were smaller and less compact compared to vehicle-treated EBs (Fig. 5G–I) (323.4 ± 64.49 μm *vs* 206.3 ± 42.66 μm; $p < 0{:}001$). Next, we wanted to determine if ESC-derived Flk1$^+$ cells play a role in graft formation past the EB formation stage. To accomplish this, we lysed Flk1$^+$ cells through Flk1 antibody complement activation prior to transplantation. Animals that were transplanted with Flk1 depleted ESC-derived NPCs ($n = 10$) did not form a graft whereas 5 out of 11 control animals that received ESC-derived NPCs without Flk1 antibody complement activation demonstrated graft formation (Table 2) indicating that Flk1$^+$ cells are essential for formation of the ESC-derived graft.

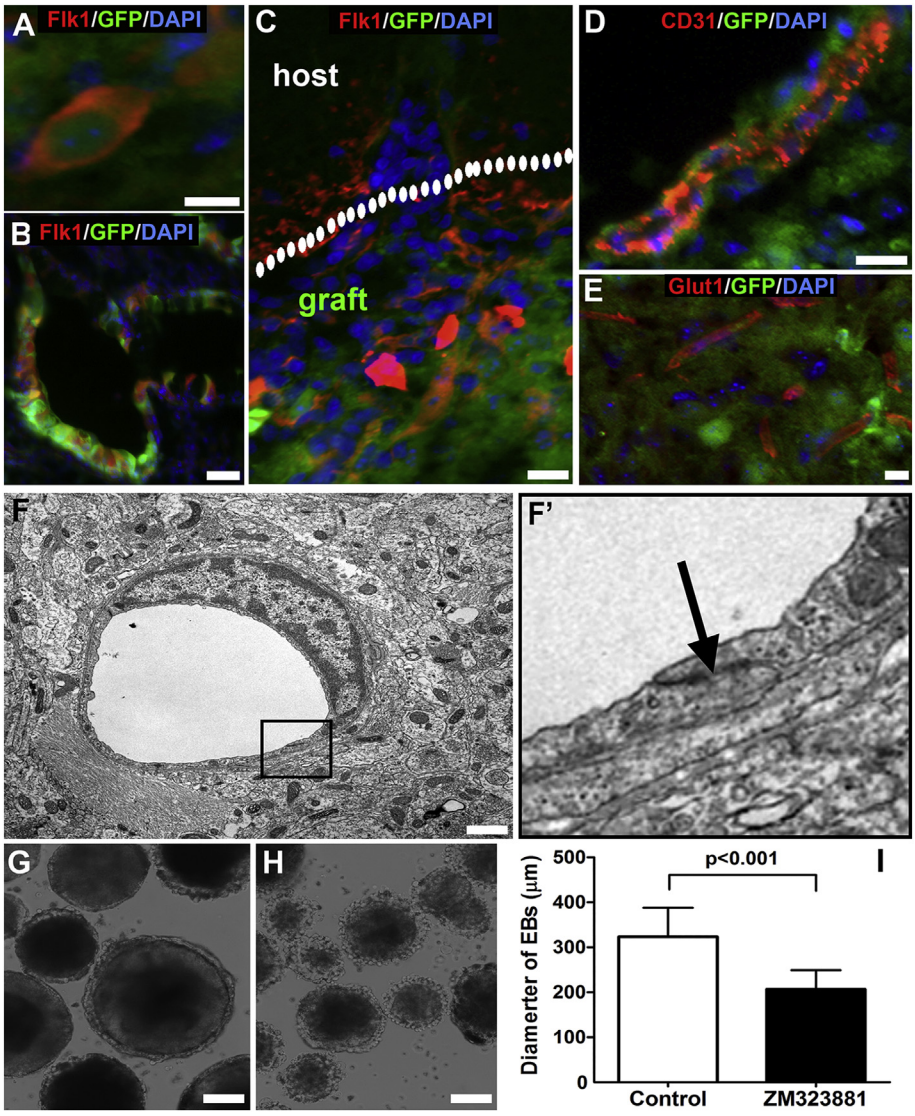

Fig. 5. Vasculogenesis in the graft. (A) GFP$^+$Flk1$^+$ cells are present in the graft as individual cells. (B) GFP$^+$Flk1$^+$ cells form vasculature in the graft. (C) Flk1$^+$ vasculature structures connect the graft with the host spinal cord. (D) GFP$^+$CD31$^+$ endothelial cells are found in the vasculature within the graft. (E) Vasculature structures in the graft express the blood-brain barrier marker Glut1. (F-F′) EM image showing formation of blood-brain barrier vasculature structures within the graft that contain tight junction formed by an endothelial cell. (G-I) Flk1 inhibitor (ZM323881) results in EBs with smaller diameters compared to non-treated EBs ($p < .001$). Scale bars: A = 10 μm; B-E = 20 μm; F = 1 μm; G-H = 100 μm.

Table 2
Summary of graft development data in animals that received ESC-derived NPC with or without depletion of Flk1$^+$ cells.

Groups	Number of animals in the group	Number of animals with graft growth	Ratio of animals with graft (%)
Control	11	5	45.5
Flk1 treated	10	0	0

4. Discussion

We validate a novel platform for studying spinal cord organogenesis that enables studies of intrinsic molecules within ESCs that drive this process, and factors within the adult spinal cord that contribute to organogenesis of the spinal cord. We show that formation of spinal cord tissue from transplanted ESC-derived NPCs can be identified through *in vivo* T2*w* MRI. The stereotypical organization of the newly formed spinal cord tissue can be determined using DTI. We went on to identify functional and anatomical features of the CNS that are formed within the newly formed spinal cord tissue. As a proof-of-concept for the utility of this platform, we demonstrate that Flk1$^+$ESC-derived cells within EBs are essential for spinal cord organogenesis. The study highlights mechanisms through which the host spinal cord can provide cues for formation of functional and anatomical features of the spinal cord.

Differentiation of ESCs into nestin$^+$NPCs has been characterized through functional gene expression (Leem et al., 2009), transcription factor profiles (Yamamizu et al., 2013), and microRNA expression profiles (Chen et al., 2010). *In vitro*, ESCs form rudimentary structures such as beating clumps of cardiac cells (Meyer et al., 2000), adenohypophysis tissue (Suga et al., 2011), and insulin secreting pancreatic islet-like cells (Lumelsky et al., 2001). However, evidence for self-organization of ESCs into organs of the CNS is limited. ESCs have been shown to self-organize into functional neural cell cultures (Lenka et al., 2002), optic cup (Eiraku et al., 2011), cortical tissue (Eiraku and Sasai, 2012), and cerebral organoids (Lancaster et al., 2013). In these reports, media with reagents and growth factors that drive lineage commitment and regional specification of cells directed self-organization and differentiation of ESCs. Using such methodology with RA as the primary inducing factor, self-organization of ESCs in tissue resembling a patterned neural tube was accomplished, and it was shown to be dependent on paracrine factors (Meinhardt et al., 2014). The strong effect of paracrine factors in self-organization of transplanted NPCs was evident in our experiments as well, where despite reducing the number of transplanted cells from the initial dose of 40 million to 2.5 million, we continued to observed graft formation. The current experiments did not.

Stereotypical self-organization of transplanted ESC-derived NPCs within the graft strongly resembled the host spinal cord stereotypical

inside-out organization with the GM on the inside being surrounded by the outside WM (Ao et al., 2011). Such self-organization of ESCs resembling a mature CNS organ was described *in vitro* where cerebral organoids resembled a mature brain (Renner et al., 2017). In case of the patterned neural tube, the self-organized organ showed early signs of neural tube formation and ventral-dorsal patterning but was not mature enough to resemble the fully formed spinal cord (Cassady et al., 2014). We confirm the stereotypical self-organization of the graft using water-diffusivity which bypasses the need for perfusion of animals without graft formation increasing the utility of this platform. In addition to the stereotypical organization, graft WM and GM contains cells with appropriate molecular phenotypes. The graft WM contained cells that had predominantly differentiated toward a glial lineage, oligodendrocytes and astrocyte while the GM predominantly had cells that were differentiated into neurons (Ao et al., 2011). Beyond the appropriate molecular phenotypes of the cells, within the graft WM, our work describes ultrastructural features of mature spinal cord such as myelinated axons and glial limitans. Differentiation of transplanted ESC-derived NPCs into oligodendrocytes in the spinal cord was previously reported (McDonald et al., 1999a). The functionality of such differentiation was confirmed in experiments where remyelination by transplanted NPCs but not shiverer NPCs (do not form compact myelin) was shown to induce recovery of motor function after spinal cord injury (SCI) (Yasuda et al., 2011). We note that despite the presence of myelinating ESC-derived oligodendrocyte, not all axons are myelinated. Such finding indicates that ESC-derived oligodendrocytes within the graft myelinate only axons with appropriate developmental signals or that some ESC-derived oligodendrocytes are not mature enough to myelinate axons. Myelination depends on neuronal activity (Demerens et al., 1996) therefore, demarcation of the paranodal regions in the axon-glial junctions by axonal localization of Caspr is an indication of developmentally appropriate neuronal activity and myelination (Einheber et al., 1997b).

The formation of another ultrastructural feature, glial limitans, was noted on the surface of the graft WM. Glia limitans is a thin protective barrier comprised of astrocytes that associate with the parenchymal basal lamina and surround the brain and spinal cord (Liu et al., 2013;Lyser, 1972). The glial limitans characterized by tight junctions was appropriately formed on the outside of the graft WM, away from the host spinal cord but not adjacent to the host spinal cord. Considering we transplanted ESC-derived NPCs adjacent to the host SCI, the glia limitans could have formed in response to signals that surrounded the graft; in turn the glial limitans formation could have preserved the graft. As a consequence of the glial limitans formation, graft ESC-derived cells did not cross the graft boundary but did cross into the host spinal cord. Differentiation of transplanted ESC-derived NPCs into astrocytes following SCI in rodents has been previously reported (Roybon et al., 2013), however, to our knowledge this is the first report that shows that newly generated astrocytes form a glial limitans.

Mouse ESCs-derived NPCs are able to further differentiate into functional neurons, *in vitro* (Bain et al., 1995;Okada et al., 2008) and *in vivo* in the spinal cord (Okada et al., 2008;McDonald et al., 1999b;Peljto et al., 2010). *In vitro,* ESC-derived neurons have tetrodotoxin-sensitive transient inward current (Na + current), and a sustained outward current (delayed rectifier K+ current). Additionally, injection of a sustained positive current induces firing of action potentials (Okada et al., 2008). *In vivo,* ESC-derived NPCs have been shown to differentiate into ChAT$^+$, GAD$^+$, 5-HT$^+$, and TH$^+$neurons that form synapses with the host neurons following transplantation in the uninjured spinal cord.(Okada et al., 2008) In this study, we confirm that ESC-derived NPCs within the graft differentiated into neurons with the same molecular phenotypes as the endogenous neurons within the host spinal cord. The presence of ChAT$^+$cholinergic motor neurons and vGlut1$^+$glutamatergic neurons is well established in the spinal cord but the presence and function of TH$^+$dopaminergic neurons, and 5-HT$^+$serotonergic neurons in the spinal cord is not as well characterized. Dopaminergic neurons have been described in the autonomic nuclei and superficial dorsal horn in L6-S3 spinal cord segments where they have modulate the bladder reflex (Hou et al., 2016). In addition to rodent spinal cord, 5-HT$^+$profiles of serotonergic neurons have been identified at the lumbar level in the ventral horn of human spinal cord where they surround motorneurons. Additionally, in human spinal cords 5-HT$^+$profiles of serotonergic neurons have been identified in the intermediolateral region, and superficial part (equivalent of Rexed lamina II) of the dorsal horn that has high levels of 5-HT(1A) receptors (Perrin et al., 2011).

Identification of factors that drive the differentiation of neurons within the graft remain to be idenfied, and is beyond the scope of this study. One possibility is that these neurons aquired their phenotype *in vitro* while another possibility is that factors within the host spinal cord drive their differentiation. Host astrocytes and axons that penetrate into the graft could enhance the survival, and drive differentiation of ESC-derived cells. In case of astrocytes this induction could be mediated by secreted factors or by cell-surface ligands (Bentz et al., 2006). However, such an inductive affect from the host CNS neurons requires formation of a functional neuronal circuitry with the graft (Song et al., 2012). Retrograde tracing confirmed that the graft forms such circuitry with the host spinal cord at lumbosacral level. An appropriate synaptic circuitry also enhances the survival of the neurons within the circuit (Buss et al., 2006); indeed ESC-derived neurons survive better once transplanted into the spinal cord if they form synapses with the host neurons (Okada et al., 2008).

Inductive effects of ESC-derived endothelial cells, and the vasculature that they form are critical in the organogenesis of the liver and pancreas (Lammert et al., 2001;Matsumoto et al., 2001). Such an effect has also been shown in the regulation of neurogenesis in the adult brain (Shen et al., 2004;Louissaint Jr. et al., 2002;Schanzer et al., 2004b). Furthermore, improved angiogensis within ischaemic tissues following a stroke induces neurogenesis and axonogenesis (Nih et al., 2018). Conversly, self-assembled grafts that contain neuronal and glial populations provide the necessary developmental cues to guide the formation of vascular networks from human ESC-derived endothelial and mesenchymal stem cells. One such cue is expression of VEGFA, a gene that associated with vascular development (Schwartz et al., 2015). We found early endothelial (Flk1$^+$) cells distributed throughout the graft as well as localized in newly formed chimeric blood vessels within the graft; therefore, Flk1$^+$cells could play a role in EB, and graft formation by exerting an inductive effect. The role of Flk1+ cells in EB formation is more complex since blocking of Flk1 kinase activity with ZM323881 is not sufficient to block RA induced EB formation; however, blocking Flk1 kinase activity results in smaller and less compact EBs. Ablation of Flk1$^+$cells after EB formation but prior to the transplantation of ESC-derived NPCs completely prevents graft formation suggesting a role for Flk1$^+$cells prior to formation of functional blood vessels. VEGF signaling through Flk1 is shared by both endothelial and NPCs where these signaling pathways control vascular, and neuronal growth and patterning (Ambler et al., 2003;Hashimoto et al., 2006;Ruiz de Almodovar et al., 2011;Sondell et al., 2000). Furthermore, NPCs can differentiate into cells of vascular and neural lineage, which leads to collaborative organogenesis (Ii et al., 2009). Indeed, Flk1 expression has been described in NPCs of adult mouse brain (Ii et al., 2009;Jin et al., 2002b) and NPCs derived from human ESCs (Reubinoff et al., 2001). It is possible that Flk1$^+$cells in EBs represent an earlier stage of neural progenitors that possess the plasticity to differentiate to other lineages (Clarke et al., 2000;Tropepe et al., 2001) including neural and endothelial cells. Moreover, induction of endothelial progenitor cells is essential for vasculogenesis that may provide 3D support and possibly organ induction and remodeling (Lammert et al., 2001;Goldberg and Hirschi, 2009;Yang et al., 2011). Inline with this, in addition to the Flk1$^+$cells within the graft (Yamaguchi et al., 1993), we note graft derived-more mature CD31$^+$endothelial cells that comprise blood vessels (Feng et al., 2004), and tight junctions of brain blood barrier

formed by Glut1$^+$endothelial cells (Engelhardt, 2003;Virgintino et al., 1997;Zheng et al., 2010). The vascular system delivers nutrients, removes waste, and may play a crucial role in the delivery of signals that regulate organ development (Lammert et al., 2001;Matsumoto et al., 2001). Therefore, our results suggest Flk1$^+$cells are important for spinal cord organogenesis possibly by acting *via* a concerted process of neurogenesis, angiogenesis, and vasculogenesis.

Implantation of human iPSC-derived cerebral organoids into a cavity made in the retrosplenial cortex of immunodeficient mice leads to the vascularization of the grafted organois (Mansour et al., 2018). Unlike the spinal cord organogenesis platform we present, the vacularization of the implanted organoids occurs exlusively from the the host vasculature by angiogenesis. Additionally, because human iPSC-derived cerebral organoids are differentiated extensively prior to implantation this model does not allow for studies of the interactions of NPCs and angiogenesis or vasculogenesis. The spinal cord organogenesis platform we present here remains the only such platform that can be used to study the effects of vasculogenesis and angiogenesis on spinal cord formation. In addition this plaform can be used to elucidate how NPC and mature neurons interact with vascular niches.

5. Conclusion

Demonstration that transplanted ESC-derived NPCs into the subarachnoid space mimic spinal cord organogenesis presents a unique platform for the study of spinal cord organogenesis. Further understanding of the factors governing this process can contribute toward development of effective therapeutic strategies for spinal cord repair. By presenting imaging methods for identification of the graft, we advance the notion that this model of spinal cord organogenesis can be used as an *in vivo* drug discovery platform for identification of novel therapeutics in regenerative medicine, and to test the toxicity of such compounds *in vivo*. As a proof-of-concept, we showed that Flk1$^+$cells are essential for the self-organization of ECS-derived NPC into spinal cord tissue.

Supplementary data to this article can be found online at https://doi.org/10.1016/j.scr.2018.09.001.

Conflicts of interest

None.

Acknowledgements

We would like to dedicate this publication to Dr. John McDonald who passed away during the submission of this manuscript. John was a friend and a colleague who inspired us to continue to pursue the research we are presenting here. He was the ultimate advocate for patients with spinal cord injuries, and a perpetual optimist. We will miss his friendship, leadership, and positive attitude. We also thank Dr. Jiangyang Zhang for help with MRI scans. We would also like to thank Dr. Lawrence Schramm for providing us with the Bartha strain of the PRV as well as technical assistance.

References

Aiba, K., Sharov, A.A., Carter, M.G., Foroni, C., Vescovi, A.L., Ko, M.S., 2006. Defining a developmental path to neural fate by global expression profiling of mouse embryonic stem cells and adult neural stem/progenitor cells. Stem Cells 24, 889–895.
Alghamdi, B., Fern, R., 2015. Phenotype overlap in glial cell populations: astroglia, oligodendroglia and NG-2(+) cells. Front. Neuroanat. 9, 49.
Ambler, C.A., Schmunk, G.M., Bautch, V.L., 2003. Stem cell-derived endothelial cells/progenitors migrate and pattern in the embryo using the VEGF signaling pathway. Dev. Biol. 257, 205–219.
Ao, H., Qu, Y., McDonald, J.W., 2011. Stem cell self-organization into mature neuronal tissue in subarachnoid space. J. Chin. Clin. Med. 6, 15–21.
Bain, G., Kitchens, D., Yao, M., Huettner, J.E., Gottlieb, D.I., 1995. Embryonic stem cells express neuronal properties in vitro. Dev. Biol. 168, 342–357.
Basso, D.M., Beattie, M.S., Bresnahan, J.C., 1995. A sensitive and reliable locomotor rating scale for open field testing in rats. J. Neurotrauma 12, 1–21.
Bentz, K., Molcanyi, M., Hess, S., Schneider, A., Hescheler, J., Neugebauer, E., Schaefer, U., 2006. Neural differentiation of embryonic stem cells is induced by signalling from non-neural niche cells. Cell. Physiol. Biochem. 18, 275–286.
Bjorklund, L.M., Sanchez-Pernaute, R., Chung, S., Andersson, T., Chen, I.Y., McNaught, K.S., Brownell, A.L., Jenkins, B.G., Wahlestedt, C., Kim, K.S., Isacson, O., 2002. Embryonic stem cells develop into functional dopaminergic neurons after transplantation in a Parkinson rat model. Proc. Natl. Acad. Sci. U. S. A. 99, 2344–2349.
Buss, R.R., Sun, W., Oppenheim, R.W., 2006. Adaptive roles of programmed cell death during nervous system development. Annu. Rev. Neurosci. 29, 1–35.
Cassady, J.P., D'Alessio, A.C., Sarkar, S., Dani, V.S., Fan, Z.P., Ganz, K., Roessler, R., Sur, M., Young, R.A., Jaenisch, R., 2014. Direct lineage conversion of adult mouse liver cells and B lymphocytes to neural stem cells. Stem Cell Reports 3, 948–956.
Chen, H., Qian, K., Tang, Z.P., Xing, B., Chen, H., Liu, N., Huang, X., Zhang, S., 2010. Bioinformatics and microarray analysis of microRNA expression profiles of murine embryonic stem cells, neural stem cells induced from ESCs and isolated from E8.5 mouse neural tube. Neurol. Res. 32, 603–613.
Clarke, D.L., Johansson, C.B., Wilbertz, J., Veress, B., Nilsson, E., Karlstrom, H., Lendahl, U., Frisen, J., 2000. Generalized potential of adult neural stem cells. Science 288, 1660–1663.
Demerens, C., Stankoff, B., Logak, M., Anglade, P., Allinquant, B., Couraud, F., Zalc, B., Lubetzki, C., 1996. Induction of myelination in the central nervous system by electrical activity. Proc. Natl. Acad. Sci. U. S. A. 93, 9887–9892.
Doevendans, P.A., Kubalak, S.W., An, R.H., Becker, D.K., Chien, K.R., Kass, R.S., 2000. Differentiation of cardiomyocytes in floating embryoid bodies is comparable to fetal cardiomyocytes. J. Mol. Cell. Cardiol. 32, 839–851.
Edlund, T., Jessell, T.M., 1999. Progression from extrinsic to intrinsic signaling in cell fate specification: A view from the nervous system. Cell 96, 211–224.
Einheber, S., Zanazzi, G., Ching, W., Scherer, S., Milner, T.A., Peles, E., Salzer, J.L., 1997a. The axonal membrane protein Caspr, a homologue of neurexin IV, is a component of the septate-like paranodal junctions that assemble during myelination. J. Cell Biol. 139, 1495–1506.
Einheber, S., Zanazzi, G., Ching, W., Scherer, S., Milner, T.A., Peles, E., Salzer, J.L., 1997b. The axonal membrane protein Caspr, a homologue of neurexin IV, is a component of the septate-like paranodal junctions that assemble during myelination. J. Cell Biol. 139, 1495–1506.
Eiraku, M., Sasai, Y., 2012. Self-formation of layered neural structures in three-dimensional culture of ES cells. Curr. Opin. Neurobiol. 22, 768–777.
Eiraku, M., Takata, N., Ishibashi, H., Kawada, M., Sakakura, E., Okuda, S., Sekiguchi, K., Adachi, T., Sasai, Y., 2011. Self-organizing optic-cup morphogenesis in three-dimensional culture. Nature 472, 51–U73.
Engelhardt, B., 2003. Development of the blood-brain barrier. Cell Tissue Res. 314, 119–129.
Feng, D., Nagy, J.A., Pyne, K., Dvorak, H.F., Dvorak, A.M., 2004. Ultrastructural localization of platelet endothelial cell adhesion molecule (PECAM-1, CD31) in vascular endothelium. J. Histochem. Cytochem. 52, 87–101.
Goldberg, J.S., Hirschi, K.K., 2009. Diverse roles of the vasculature within the neural stem cell niche. Regen. Med. 4, 879–897.
Hashimoto, T., Zhang, X.M., Chen, B.Y., Yang, X.J., 2006. VEGF activates divergent intracellular signaling components to regulate retinal progenitor cell proliferation and neuronal differentiation. Development (133), 2201–2210.
Hou, S., Carson, D.M., Wu, D., Klaw, M.C., Houle, J.D., Tom, V.J., 2016. Dopamine is produced in the rat spinal cord and regulates micturition reflex after spinal cord injury. Exp. Neurol. 285, 136–146.
Ii, M., Nishimura, H., Sekiguchi, H., Kamei, N., Yokoyama, A., Horii, M., Asahara, T., 2009. Concurrent vasculogenesis and neurogenesis from adult neural stem cells. Circ. Res. 105, 860–868.
Jiang, H., van Zijl, P.C., Kim, J., Pearlson, G.D., Mori, S., 2006. DtiStudio: resource program for diffusion tensor computation and fiber bundle tracking. Comput. Methods Prog. Biomed. 81, 106–116.
Jin, K.L., Zhu, Y.H., Sun, Y.J., Mao, X.O., Xie, L., Greenberg, D.A., 2002a. Vascular endothelial growth factor (VEGF) stimulates neurogenesis in vitro and in vivo. Proc. Natl. Acad. Sci. U. S. A. 99, 11946–11950.
Jin, K., Zhu, Y., Sun, Y., Mao, X.O., Xie, L., Greenberg, D.A., 2002b. Vascular endothelial growth factor (VEGF) stimulates neurogenesis in vitro and in vivo. Proc. Natl. Acad. Sci. U. S. A. 99, 11946–11950.
Kabrun, N., Buhring, H.J., Choi, K., Ullrich, A., Risau, W., Keller, G., 1997. Flk-1 expression defines a population of early embryonic hematopoietic precursors. Development 124, 2039–2048.
Kaufman, D.S., Hanson, E.T., Lewis, R.L., Auerbach, R., Thomson, J.A., 2001. Hematopoietic colony-forming cells derived from human embryonic stem cells. Proc. Natl. Acad. Sci. U. S. A. 98, 10716–10721.
Klug, M.G., Soonpaa, M.H., Koh, G.Y., Field, L.J., 1996. Genetically selected cardiomyocytes from differentiating embronic stem cells form stable intracardiac grafts. J. Clin. Invest. 98, 216–224.
Kuhnert, F., Mancuso, M.R., Shamloo, A., Wang, H.T., Choksi, V., Florek, M., Su, H., Fruttiger, M., Young, W.L., Heilshorn, S.C., Kuo, C.J., 2010. Essential regulation of CNS angiogenesis by the orphan G protein-coupled receptor GPR124. Science 330, 985–989.
Lammert, E., Cleaver, O., Melton, D., 2001. Induction of pancreatic differentiation by signals from blood vessels. Science 294, 564–567.
Lancaster, M.A., Renner, M., Martin, C.A., Wenzel, D., Bicknell, L.S., Hurles, M.E., Homfray, T., Penninger, J.M., Jackson, A.P., Knoblich, J.A., 2013. Cerebral organoids model human brain development and microcephaly. Nature 501, 373–379.
Lee, S.H., Lumelsky, N., Studer, L., Auerbach, J.M., McKay, R.D., 2000. Efficient

generation of midbrain and hindbrain neurons from mouse embryonic stem cells. Nat. Biotechnol. 18, 675–679.
Leem, S.H., Ahn, E.K., Heo, J., 2009. Functional classification of gene expression profiles during differentiation of mouse embryonic cells on monolayer culture. Animal Cells Syst. 13, 235–245.
Lenka, N., Lu, Z.J., Sasse, P., Hescheler, J., Fleischmann, B.K., 2002. Quantitation and functional characterization of neural cells derived from ES cells using nestin enhancer-mediated targeting in vitro. J. Cell Sci. 115, 1471–1485.
Liu, S., Qu, Y., Stewart, T.J., Howard, M.J., Chakrabortty, S., Holekamp, T.F., McDonald, J.W., 2000. Embryonic stem cells differentiate into oligodendrocytes and myelinate in culture and after spinal cord transplantation. Proc. Natl. Acad. Sci. U. S. A. 97, 6126–6131.
Liu, X., Zhang, Z., Guo, W., Burnstock, G., He, C., Xiang, Z., 2013. The superficial glia limitans of mouse and monkey brain and spinal cord. Anat. Rec. (Hoboken) 296, 995–1007.
Louissaint Jr., A., Rao, S., Leventhal, C., Goldman, S.A., 2002. Coordinated interaction of neurogenesis and angiogenesis in the adult songbird brain. Neuron 34, 945–960.
Lumelsky, N., Blondel, O., Laeng, P., Velasco, I., Ravin, R., McKay, R., 2001. Differentiation of embryonic stem cells to insulin-secreting structures similar to pancreatic islets. Science 292, 1389–1394.
Lyser, K.M., 1972. The differentiation of glial cells and glia limitans in organ cultures of chick spinal cord. In Vitro 8, 77–84.
Mansour, A.A., Goncalves, J.T., Bloyd, C.W., Li, H., Fernandes, S., Quang, D., Johnston, S., Parylak, S.L., Jin, X., Gage, F.H., 2018. An in vivo model of functional and vascularized human brain organoids. Nat. Biotechnol. 36, 432–441.
Matsumoto, K., Yoshitomi, H., Rossant, J., Zaret, K.S., 2001. Liver organogenesis promoted by endothelial cells prior to vascular function. Science 294, 559–563.
McDonald, J.W., Liu, X.Z., Qu, Y., Liu, S., Mickey, S.K., Turetsky, D., Gottlieb, D.I., Choi, D.W., 1999a. Transplanted embryonic stem cells survive, differentiate and promote recovery in injured rat spinal cord. Nat. Med. 5, 1410–1412.
McDonald, J.W., Liu, X.Z., Qu, Y., Liu, S., Mickey, S.K., Turetsky, D., Gottlieb, D.I., Choi, D.W., 1999b. Transplanted embryonic stem cells survive, differentiate and promote recovery in injured rat spinal cord. Nat. Med. 5, 1410–1412.
Meinhardt, A., Eberle, D., Tazaki, A., Ranga, A., Niesche, M., Wilsch-Brauninger, M., Stec, A., Schackert, G., Lutolf, M., Tanaka, E.M., 2014. 3D Reconstitution of the Patterned Neural Tube from Embryonic Stem Cells. Stem Cell Rep. 3, 987–999.
Meyer, N., Jaconi, M., Landopoulou, A., Fort, P., Puceat, M., 2000. A fluorescent reporter gene as a marker for ventricular specification in ES-derived cardiac cells. FEBS Lett. 478, 151–158.
Nih, L.R., Gojgini, S., Carmichael, S.T., Segura, T., 2018. Dual-function injectable angiogenic biomaterial for the repair of brain tissue following stroke. Nat. Mater. 17 (7), 642–651.
Okada, Y., Matsumoto, A., Shimazaki, T., Enoki, R., Koizumi, A., Ishii, S., Itoyama, Y., Sobue, G., Okano, H., 2008. Spatiotemporal recapitulation of central nervous system development by murine embryonic stem cell-derived neural stem/progenitor cells. Stem Cells 26, 3086–3098.
Palacios, R., Golunski, E., Samaridis, J., 1995. In vitro generation of hematopoietic stem cells from an embryonic stem cell line. In: Proceedings of the National Academy of Sciences of the United States of America. vol. 92. pp. 7530–7534.
Pan, B.H., Kim, E.J., Schramm, L.P., 2005. Increased close appositions between corticospinal tract axons and spinal sympathetic neurons after spinal cord injury in rats. J. Neurotrauma 22, 1399–1410.
Peljto, M., Dasen, J.S., Mazzoni, E.O., Jessell, T.M., Wichterle, H., 2010. Functional diversity of ESC-derived motor neuron subtypes revealed through intraspinal transplantation. Cell Stem Cell 7, 355–366.
Perrin, F.E., Gerber, Y.N., Teigell, M., Lonjon, N., Boniface, G., Bauchet, L., Rodriguez, J.J., Hugnot, J.P., Privat, A.M., 2011. Anatomical study of serotonergic innervation and 5-HT(1A) receptor in the human spinal cord. Cell Death Dis. 2, e218.
Renner, M., Lancaster, M.A., Bian, S., Choi, H., Ku, T., Peer, A., Chung, K., Knoblich, J.A., 2017. Self-organized developmental patterning and differentiation in cerebral organoids. EMBO J. 36, 1316–1329.
Reubinoff, B.E., Itsykson, P., Turetsky, T., Pera, M.F., Reinhartz, E., Itzik, A., Ben-Hur, T., 2001. Neural progenitors from human embryonic stem cells. Nat. Biotechnol. 19, 1134–1140.
Roybon, L., Lamas, N.J., Garcia-Diaz, A., Yang, E.J., Sattler, R., Jackson-Lewis, V., Kim, Y.A., Kachel, C.A., Rothstein, J.D., Przedborski, S., Wichterle, H., Henderson, C.E., 2013. Human stem cell-derived spinal cord astrocytes with defined mature or reactive phenotypes. Cell Rep. 4, 1035–1048.
Ruiz De Almodovar, C., Fabre, P.J., Knevels, E., Coulon, C., Segura, I., Haddick, P.C., Aerts, L., Delattin, N., Strasser, G., Oh, W.J., Lange, C., Vinckier, S., Haigh, J., Fouquet, C., Gu, C., Alitalo, K., Castellani, V., Tessier-Lavigne, M., Chedotal, A., Charron, F., Carmeliet, P., 2011. VEGF mediates commissural axon chemoattraction through its receptor Flk1. Neuron 70, 966–978.
Schanzer, A., Wachs, F.P., Wilhelm, D., Acker, T., Cooper-Kuhn, C., Beck, H., Winkler, J., Aigner, L., Plate, K.H., Kuhn, H.G., 2004a. Direct stimulation of adult neural stem cells in vitro and neurogenesis in vivo by vascular endothelial growth factor. Brain Pathol. 14, 237–248.
Schanzer, A., Wachs, F.P., Wilhelm, D., Acker, T., Cooper-Kuhn, C., Beck, H., Winkler, J., Aigner, L., Plate, K.H., Kuhn, H.G., 2004b. Direct stimulation of adult neural stem cells in vitro and neurogenesis in vivo by vascular endothelial growth factor. Brain Pathol. 14, 237–248.
Schwartz, M.P., Hou, Z., Propson, N.E., Zhang, J., Engstrom, C.J., Santos Costa, V., Jiang, P., Nguyen, B.K., Bolin, J.M., Daly, W., Wang, Y., Stewart, R., Page, C.D., Murphy, W.L., Thomson, J.A., 2015. Human pluripotent stem cell-derived neural constructs for predicting neural toxicity. Proc. Natl. Acad. Sci. U. S. A. 112, 12516–12521.
Shen, Q., Goderie, S.K., Jin, L., Karanth, N., Sun, Y., Abramova, N., Vincent, P., Pumiglia, K., Temple, S., 2004. Endothelial cells stimulate self-renewal and expand neurogenesis of neural stem cells. Science 304, 1338–1340.
Sondell, M., Sundler, F., Kanje, M., 2000. Vascular endothelial growth factor is a neurotrophic factor which stimulates axonal outgrowth through the flk-1 receptor. Eur. J. Neurosci. 12, 4243–4254.
Song, J., Zhong, C., Bonaguidi, M.A., Sun, G.J., Hsu, D., Gu, Y., Meletis, K., Huang, Z.J., Ge, S., Enikolopov, G., Deisseroth, K., Luscher, B., Christian, K.M., Ming, G.L., Song, H., 2012. Neuronal circuitry mechanism regulating adult quiescent neural stem-cell fate decision. Nature 489, 150–154.
Suga, H., Kadoshima, T., Minaguchi, M., Ohgushi, M., Soen, M., Nakano, T., Takata, N., Wataya, T., Muguruma, K., Miyoshi, H., Yonemura, S., Oiso, Y., Sasai, Y., 2011. Self-formation of functional adenohypophysis in three-dimensional culture. Nature 480, 57–62.
Tropepe, V., Hitoshi, S., Sirard, C., Mak, T.W., Rossant, J., van der Kooy, D., 2001. Direct neural fate specification from embryonic stem cells: a primitive mammalian neural stem cell stage acquired through a default mechanism. Neuron 30, 65–78.
Virgintino, D., Robertson, D., Monaghan, P., Errede, M., Bertossi, M., Ambrosi, G., Roncali, L., 1997. Glucose transporter GLUT1 in human brain microvessels revealed by ultrastructural immunocytochemistry. J. Submicrosc. Cytol. Pathol. 29, 365–370.
Wichterle, H., Lieberam, I., Porter, J.A., Jessell, T.M., 2002. Directed differentiation of embryonic stem cells into motor neurons. Cell 110, 385–397.
Xiao, Z., Kong, Y., Yang, S., Li, M., Wen, J., Li, L., 2007. Upregulation of Flk-1 by bFGF via the ERK pathway is essential for VEGF-mediated promotion of neural stem cell proliferation. Cell Res. 17, 73–79.
Yamaguchi, T.P., Dumont, D.J., Conlon, R.A., Breitman, M.L., Rossant, J., 1993. flk-1, an flt-related receptor tyrosine kinase is an early marker for endothelial cell precursors. Development 118, 489–498.
Yamamizu, K., Piao, Y., Sharov, A.A., Zsiros, V., Yu, H., Nakazawa, K., Schlessinger, D., Ko, M.S., 2013. Identification of transcription factors for lineage-specific ESC differentiation. Stem Cell Rep. 1, 545–559.
Yamashita, J., Itoh, H., Hirashima, M., Ogawa, M., Nishikawa, S., Yurugi, T., Naito, M., Nakao, K., Nishikawa, S., 2000. Flk1-positive cells derived from embryonic stem cells serve as vascular progenitors. Nature 408, 92–96.
Yang, X.T., Bi, Y.Y., Feng, D.F., 2011. From the vascular microenvironment to neurogenesis. Brain Res. Bull. 84, 1–7.
Yasuda, A., Tsuji, O., Shibata, S., Nori, S., Takano, M., Kobayashi, Y., Takahashi, Y., Fujiyoshi, K., Hara, C.M., Miyawaki, A., Okano, H.J., Toyama, Y., Nakamura, M., Okano, H., 2011. Significance of remyelination by neural stem/progenitor cells transplanted into the injured spinal cord. Stem Cells 29, 1983–1994.
Zheng, P.P., Romme, E., van der Spek, P.J., Dirven, C.M., Willemsen, R., Kros, J.M., 2010. Glut1/SLC2A1 is crucial for the development of the blood-brain barrier in vivo. Ann. Neurol. 68, 835–844.